REGULAR PAPER

Real Time Water Contents Measurement Based on Step Response for PEM Fuel Cell

Dong-Hoon Shin[1] · Seung-Ryeol Yoo[1] · Young-Hyun Lee[2]

Abstract

This paper proposes a real time monitoring method of the status of flooding and drying out of a proton exchange membrane in a Polymer Electrolyte Membrane Fuel Cell (PEMFC). The PEMFC stack is modeled using the simplified Randle's equivalent electrical circuit. The measured stack voltages after a step current consumption provides the criterion for the water balance condition in the PEMFC. The voltage response has different characteristics in drying out and flooding conditions and it is possible to find membrane resistance and activation resistance corresponding to the equivalent circuit model. Since these resistance elements show a different behavior in each of the water balance states, it is possible to judge the water balance condition in the PEMFC. Furthermore, this method requires no additional costly equipment and needs only simple signal processing. The proposed method is applied to a PEMFC stack operating in normal, drying, and flooding conditions, with the results verifying that the new method can monitor the water contents of the stack.

Keywords Step response · Polymer electrolyte membrane fuel cell · Water contents · Dry-out · Flooding

List of Symbols

A_c	Catalyst specific area, cm^2/mg
a	Transfer coefficient
BOP	Balance of plant
C	Double layer capacitance
E_c	Activation energy, 66 kJ/mol
F	Faraday's constant, 96,487 C/mole pressure
h	Relative humidity of reactants
I	Current density, A/cm^2
I_0	Exchange current density, A/cm^2
K	Ion conductivity
L_c	Catalyst loading, mg/cm^2
μ	Number of moles of a water molecule compared to SO_3^- in electrolyte membrane
n	Number of electron per molecule of hydrogen, 2
P	Pressure, kPa
R_a	Activation resistance
R_m	Membrane resistance
R_u	Universal gas constant, 8.314 J/mol/K
T	Temperature, K
t	Thickness of electrolyte membrane
V_R	Voltage drop by membrane resistance
V_C	Voltage drop by membrane and double layer capacitance parallel circuit
α	Initial voltage value for the given step current, α
β	Initial current value

✉ Seung-Ryeol Yoo
  yoos@koreatech.ac.kr

1 School of Mechanical Engineering, Korea University of Technology and Education, 1600, Chungjeol-ro, Byeongcheon-myeon, Dongnam-gu, Cheonan-Si, Chungcheongnam-do 31253, Republic of Korea

2 Department of Electronic Engineering, Kangnam University, 40, Gangnam-ro, Giheung-gu, Yongin-Si, Gyeonggi-do 16979, Republic of Korea

1 Introduction

Growing concerns about the maleficence and finite quantity of fossil fuel resources has increased public attention toward fuel cells as a next-generation power source. The noteworthy advantages, including low-operating temperature, high efficiency, and high power density, have made fuel cells an important contender as an alternative power source.

As PEMFCs near commercialization, precise fault diagnosis methods to promote stable stacks and robust performance are playing an increasingly essential role. Some diagnosis methods use the well-known Electrochemical Impedance Spectroscopy (EIS) based on a small sinusoidal perturbation within a frequency range [1, 2]. Some diagnosis methods

measure cell voltage [3] and frequency distortion [4] to detect abnormal states.

Appropriate hydration of a fuel cell stack is becoming a more significant issue because cell flooding or membrane drying, which degrade fuel cell energy generation, occurs frequently during fuel cell operation. Therefore, diagnosis methods monitoring the conditions related to water balance have been developed. One such method involves measuring the AC impedance using EIS with equivalent circuit models [5, 6]. In addition, neural network modeling has been used to diagnose water balance failure in PEMFCs [7], and fault tolerant control strategies have been implemented to monitor the SOH of the stack [8]. Although these provide precise stack condition parameters, they are difficult to apply online because the EIS method is based on various sinusoidal perturbations off-line, and signal processing required costly and heavy instruments.

This paper proposes a Step Response Analysis (SRA) based on the simplified Randle's circuit, monitoring the flooding or drying out condition of the PEMFC. Occurrence of the drying out state leads to the degradation of the proton exchange efficiency of the electrolyte membrane in the Membrane Electrolyte Assembly (MEA), which is related to resistance polarization caused by Rm. On the other hand, under flooding conditions the Gas Diffusion Layer (GDL) is filled with water droplets which hinder approach of reactants to the catalyst area on the MEA, eventually giving rise to polarization related to Ra. The initial voltage response by step input current is related to membrane resistance and the final voltage response is related to activation resistance. By calculating and comparing these resistance values, the water content conditions in PEMFC can be monitored.

2 Step Response Analysis

2.1 Mathematical Expression of Step Response

The proposed step response analysis is a method where the membrane resistance, the activation resistance, and the double layer capacitance of the equivalent circuit of the PEMFC can be measured after a step current consumption is applied to the stack. A fuel cell stack can consist of between a few to hundreds of fuel cells, 400 fuel cells being common in automobile applications. Only measured stack voltage and current values are used for monitoring in this paper and the simplified Randle's equivalent circuit shown in Fig. 1 is the chosen model for the SRA method.

In Fig. 1, circuit current i(t) and circuit voltage can be defined as Eqs. (1) and (2).

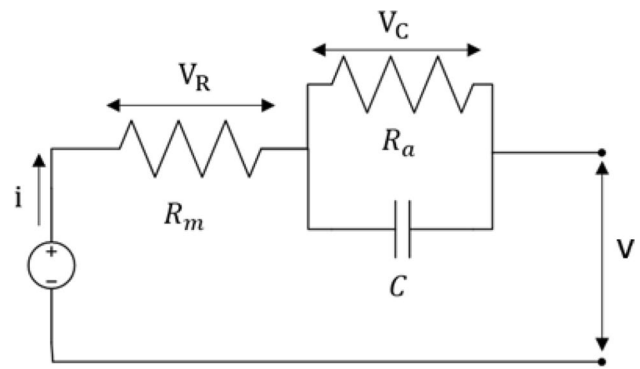$$i(t) = C\frac{dV_c(t)}{dt} + \frac{V_c(t)}{R_a} \tag{1}$$

Fig. 1 Simplified randles equivalent circuit

$$V(t) = V_R(t) + V_c(t) = i(t)R_m + V_c(t) \tag{2}$$

System Eqs. (1) and (2) are combined and can be written as follows.

$$\frac{dV(t)}{dt} + \frac{1}{CR_a}V(t) = i(t)\left(\frac{R_a + R_m}{CR_a}\right) + R_m\frac{di(t)}{dt} \tag{3}$$

By applying the Laplace transform (3) and letting the initial conditions of voltage and current be α and β, respectively, $V(S)$ is obtained as Eq. (5).

$$SV(S) + \frac{1}{CR_a}V(S) - v(0^-) = \frac{R_a + R_m}{CR_a}I(S) + R_m SI(S) - R_m i(0^-) \tag{4}$$

$$V(S) = \frac{\alpha - R_m\beta}{S + \frac{1}{CR_a}} + \left\{R_m - \frac{\frac{R_m}{CR_a} - \bar{C}}{S + \frac{1}{CR_a}}\right\}I(S) \tag{5}$$

Here, $\bar{C}$ is $\frac{R_a + R_m}{CR_a}$.

In order to find the output voltage v(t) from Eq. (5), the inverse Laplace transform can be applied to Eq. (5).

$$V(t) = L^{-1}\left(\frac{\alpha - R_m\beta}{S + \frac{1}{CR_a}}\right) + L^{-1}\left(\left\{R_m - \frac{\frac{R_m}{CR_a} - \bar{C}}{S + \frac{1}{CR_a}}\right\}I(S)\right). \tag{6}$$

The first term is easily obtained with $(\alpha - R_m\beta)e^{-\frac{t}{CR_a}}$. The second term can be solved using the convolution operation as shown in Eq. (7).

$$L^{-1}\left(R_m - \frac{\frac{R_m}{CR_a} - \bar{C}}{S + \frac{1}{CR_a}}I(S)\right) = R_m i(t) - \left(\frac{R_m}{R_a} - \bar{C}\right)\int_0^t e^{-\frac{t-\sigma}{CR_a}}i(\sigma)d\sigma \tag{7}$$

The current i(t) used for step consuming is modeled as shown in Fig. 2 and can be expressed as i(t) = $\beta - u(t - t_0)$.
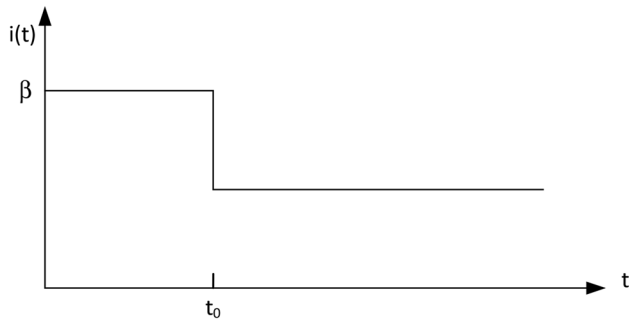
Fig. 2 Current step shape for the model

For the current step model, the integral term in Eq. (7) is as follows.

$$\int_0^t e^{-\frac{t-\sigma}{CR_a}} i(\sigma)d\sigma = \int_0^{t_0} e^{-\frac{t-\sigma}{CR_a}}\beta d\sigma + \int_{t_0}^t e^{-\frac{t-\sigma}{CR_a}}(\beta-1)d\sigma$$

$$= \beta CR_a\left(e^{\frac{t_0-t}{CR_a}} - e^{-\frac{t}{CR_a}}\right)$$

$$+ (\beta-1)CR_a\left(1 - e^{\frac{t_0-t}{CR_a}}\right)$$

The final output voltage V(t) is as follows.

$$V(t) = (\alpha - R_m\beta)e^{-\frac{t}{CR_a}} + R_m\{\beta - u(t-t_0)\}$$
$$- \beta R_a\left(e^{\frac{t_0-t}{CR_a}} - e^{-\frac{t}{CR_a}}\right)$$
$$+ (\beta-1)R_a\left(1 - e^{\frac{t_0-t}{CR_a}}\right) \tag{8}$$

The output voltage may be simplified if the start time, t_0, of the step input is zero, as follows.

$$V(t) = (\alpha - R_m\beta)e^{-\frac{t}{CR_a}} + R_m\{\beta - u(t)\} + (\beta-1)R_a\left(1 - e^{-\frac{t}{CR_a}}\right) \tag{9}$$

If we focus on the value of V(t) when $t = 0^+$ and $t = \infty$, the following is derived.

$$V(0^+) = \alpha - R_m\beta + R_m\beta - R_m = \alpha - R_m$$

$$V(\infty) = R_m\beta - R_m + R_a\beta - R_a = (\beta-1)(R_m + R_a) \tag{10}$$

From the conditions of Eq. (10), membrane resistance R_m and activation resistance R_a can be calculated.

$$V(0^-) - V(0^+) = \alpha - (\alpha - R_m) = R_m$$

$$V(0^-) - V(\infty) = \beta(R_m + R_a) - (\beta-1)(R_m + R_a) = R_m + R_a \tag{11}$$

2.2 Simulation of Step Response

Based on Sect. 2.1, the simulation is conducted under the condition shown in Table 1 to prove if SRA is useful for finding R_m, R_a, and C in a PEMFC. In the simulation, the

Table 1 Simulation condition of SRA

Parameters	Unit	Values
R_m membrane resistance	Ω	0.008
R_a activation resistance	Ω	0.012
C double layer capacitance	F	1.75
α current magnitude	A	1
fs, sampling frequency	kHz	10

unit step signal is imposed at $t = 0$ as a unit current load command and Fig. 3 shows the voltage response of the stack simulator. The initial stack voltage response shows R_m at $t = 0$ and the final response shows $R_m + R_a$ at t≈∞. Thus, through the simulation of the theoretical expression of SRA, it's demonstrated that SRA is valid for finding R_m, R_a and C.

3 Experimental Setup

3.1 System Layout

The main components of the PEMFC test bench are a hydrogen tank, an air compressor mass flow controllers, humidifiers, two xPC targets and an electric load to consume current. The two xPC targets are based on the Matlab© real time controller and one xPC is for the stack control and the other for fast data measurement.

The specification of the stack is listed in Table 2, and the output graph of the fuel cell used in the experiment is shown in Fig. 4. The schematic diagram of the system is shown in Fig. 5. The heating and cooling system for the stack is installed to control the stack temperature for each status. In addition, another heating and cooling system controls the temperature of two humidifiers of H_2 and O_2.
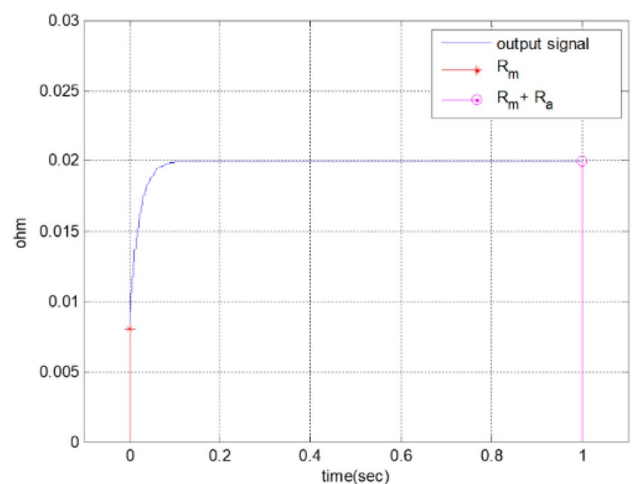

Fig. 3 Variation of R_m and R_a in simulation

Table 2 Specification of PEMFC used in this test

Items	Unit	Specification
Power	W	75
Number of cells		5
Active cell area	cm^2	25
Maximum current at normal operation	A/cm^2	1
Open circuit voltage	V	4.75
Nominal voltage	V	3.0~3.5
Minimum voltage	V	2.0 @ dry media (air/H$_2$)
Membrane electrode assembly	–	Gore® M725
Gas diffusion layer	–	SIGRACET® GDL10BC
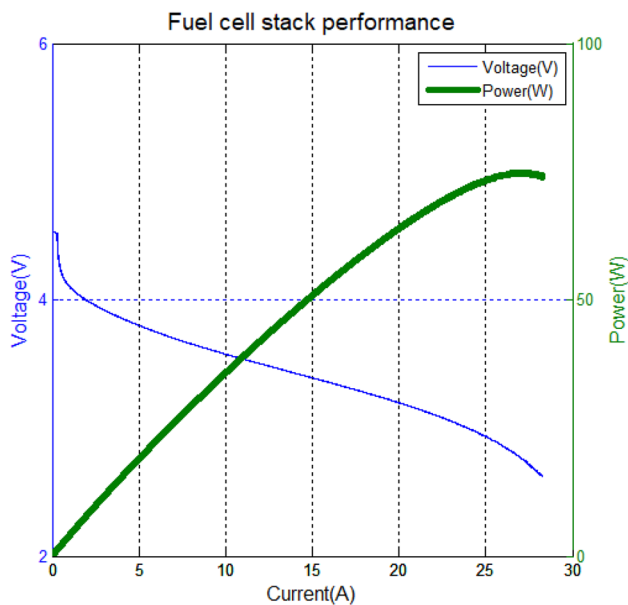
Fig. 4 Measured fuel cell stack output

3.2 Experimental Conditions

3.2.1 Fuel Cell Operating Conditions

For fuel cell operation, H$_2$ and air are supplied to the system 1.5~2 times more than stoichiometric fuel-to-oxidizer consumption and that changes linearly according to current consumption. Thus, 2 LPM H$_2$ and 6 LPM air are constantly supplied regardless of test states and considering the losses of the system. Also, back pressure and remaining fuel and air which affect PEMFC performance are emitted only at atmospheric pressure during the experiment. The 99.999% purity hydrogen and dry air controlled by the mass flow controller are humidified in the bubble type humidifier. The fuel

and air are heated or cooled before supplying to the PEMFC according to test states shown in Table 3.

The operation point, 0.6A/cm^2(15A), is selected in the linear section of the performance curve of the PEMFC. The linear range of the performance curve is normal operation section of the fuel cell. Any point included in the normal operating range can be used as an operation point, but we selected this operation point considering the performance of BOP. Also, we set the current step magnitude to 0.04A/cm^2(1A) because it is convenient for assigning to the formula, and is useful for intuitively observing the experimental results.

3.2.2 Optimization of Sampling Frequency

As discussed before, the initial response of PEMFC for a step response is the most important point to obtain the time constant and R_m of the PEMFC. However, the ideal initial response at $t = 0$ is impossible to measure using any practical devices. The ideal sampling frequency should be as high as possible, but practical devices cannot have boundless memory space or infinitely high sampling frequency. Thus, several tests under steady-state conditions as shown in Table 4 were conducted to find the proper sampling frequency, considering the performance of Data Acquisition (DAQ) devices and target xPCs. After investigating the step response according to the various sampling frequencies, almost the same gradients of each response are shown on the data sampled from 10 to 25 kHz as shown in Fig. 6. Based on these tests, 10 kHz sampling frequency is selected to acquire the initial response of PEMFC stack and to have enough memory space.

3.3 Experimental Results

3.3.1 State 1 (Dry Out Condition)

The relative humidity of H$_2$ and air are decreasing as temperatures are changed from 60 to 30 °C so that the stack is controlled to reach the dry-out state gradually. In Fig. 7, the additional polarization of the fuel cell stack compared to initial condition can be identified. More precisely, the stack performs 3.425 V at 300 s but when dry-out state is proceeding, it shows 3.189 V, which is 7.6% lower than the initial state at 2000 s. The experiment during each state is conducted 16 times, and 15 data except the first data of each state are considered as valuable data. In the Fig. 8, the membrane resistance and the activation resistance are calculated and shown to increase during State 1. Table 5 shows the transition of the R_a, R_m showing 25.35% and 49.45%, finally increasing respectively.
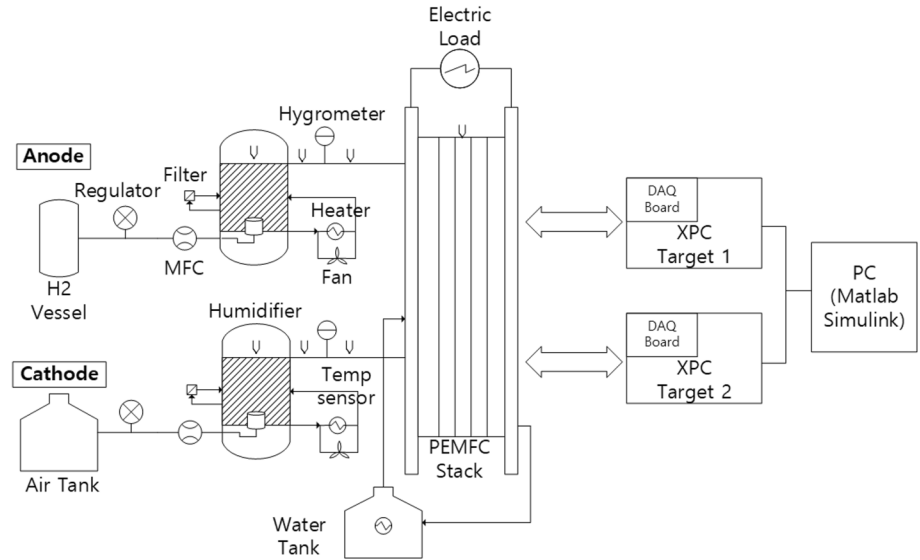
Fig. 5 Schematic diagram of PEMFC test bench

Table 3 Test conditions of each test state

Items	Unit	State conditions		
		State 1 (dry condition)	State 2 (back to normal)	State 3 (flooding condition)
H2 flow rate	LPM	2	2	2
Air flow rate	LPM	6	6	6
Temperature at H2 humidifier	°C	60→30	30→60	60→70
Temperature at air humidifier	°C	60→30	30→60	60→70
Temperature at pipe	°C	60	60	60
Temperature at stack	°C	60	60	60
DC current consumption	A/cm^2	0.6	0.6	0.6
Step magnitude	A/cm^2	0.04	0.04	0.04
Test time	sec	2000	2000	2000
Input signal cycle	sec	120	120	120
Input signal duty ratio	%	2.5	2.5	2.5

Table 4 Test conditions for sampling frequency optimization

Items	Unit	Conditions
H$_2$ relative humidity	%	60~64
Air relative humidity	%	99
H$_2$ flow rate	LPM	2
Air flow rate	LPM	6
Temperature at stack	°C	60
DC current	A/cm^2	15
Step magnitude	A/cm^2	1
Test frequency	kHz	1,2,5,8,10,20,25

3.3.2 State 2 (Back to Normal Condition)

State 2 aims to restore the fuel cell stack condition to normal state and observe perturbation during that process. For restoration of fuel cell stack conditions, the water of each humidifier is re-heated to 60 °C, the same as the initial state. In this
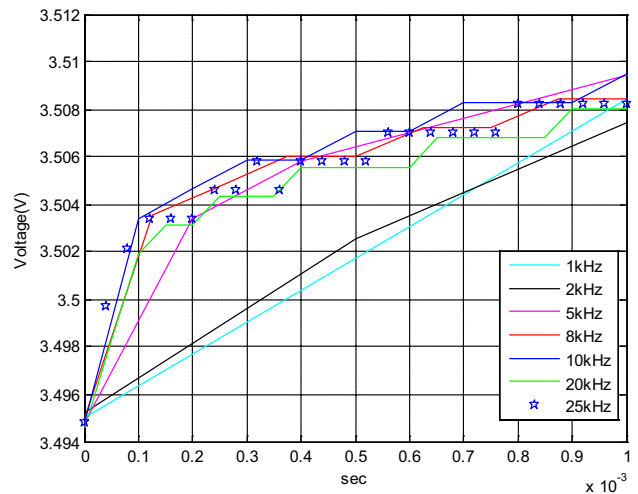

Fig. 6 Step response by different sampling frequencies

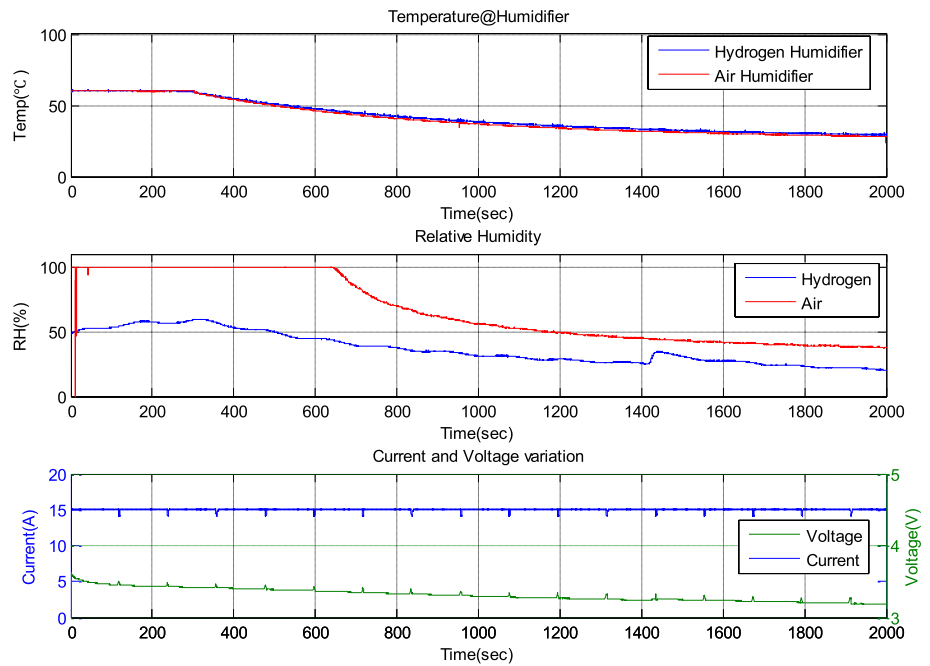**Fig. 7** Trends of several important conditions of test bench during State 1

Table 5 Transition of the resistance parameters during State 1

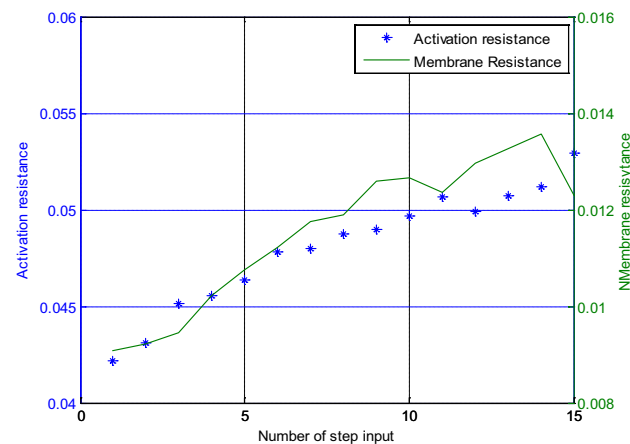| No. of sampled data	R_a	R_m
Experiment 1	0.0422	0.0091
Experiment 4	0.0455	0.0102
Experiment 8	0.0488	0.0119
Experiment 12	0.0499	0.0130
Experiment 15	0.0529	0.0136
Δ Total (%)	+ 25.35	+ 49.45

Fig. 8 Variation of activation and membrane resistance of the stack during State 1

state, as expected, all parameters composing simplified Randle's cell are changing reversely to State 1. Figures 9 and 10 represents the change of fuel cell stack conditions and each

parameter. In Table 6, R_a is restored to the conditions before the start of State1 and R_m is decreased a little far from the initial condition that the fuel cell had before the start of State1.

3.3.3 State 3 (Flooding Condition)

State 3 starts from the steady-state operation to the flooding condition by heating the water of the humidifier to 80 °C while maintaining temperatures of the stack, pipe, and other parts that constitute the supply path of fuel and air to the stack at 60 °C. The variation of some important operating conditions during State 3 is shown in Fig. 11. Table 7 shows that R_a exhibits outstanding increases of about 51% and R_m is decreased to − 15.85% and these results can be seen in Fig. 12.

The overall change of the membrane resistance and the activation resistance according to each state is shown in Fig. 13. As noted earlier, the membrane resistance corresponding to the dry-out shows a large change (up to 49.45%); however, the amount of change in the membrane resistance beyond State 2 is getting smaller and converges to the constant value. In State 3, the membrane resistance is decreased up to 14.63%. The activation resistance showed a small increase in the dry-out state, a little change in State 2, and a dramatic increase up to 50.32% during the flooding conditions.

4 Analysis of Experimental Results

4.1 Analysis of State 1

The dry-out condition leads to an increase in resistance polarization by degrading the H⁺ ionic conductivity of polymer

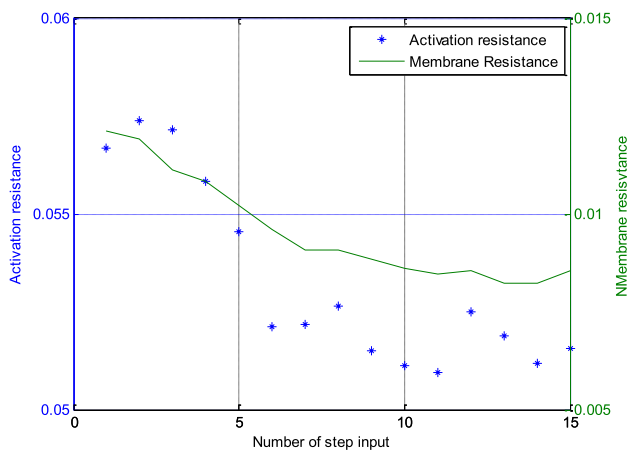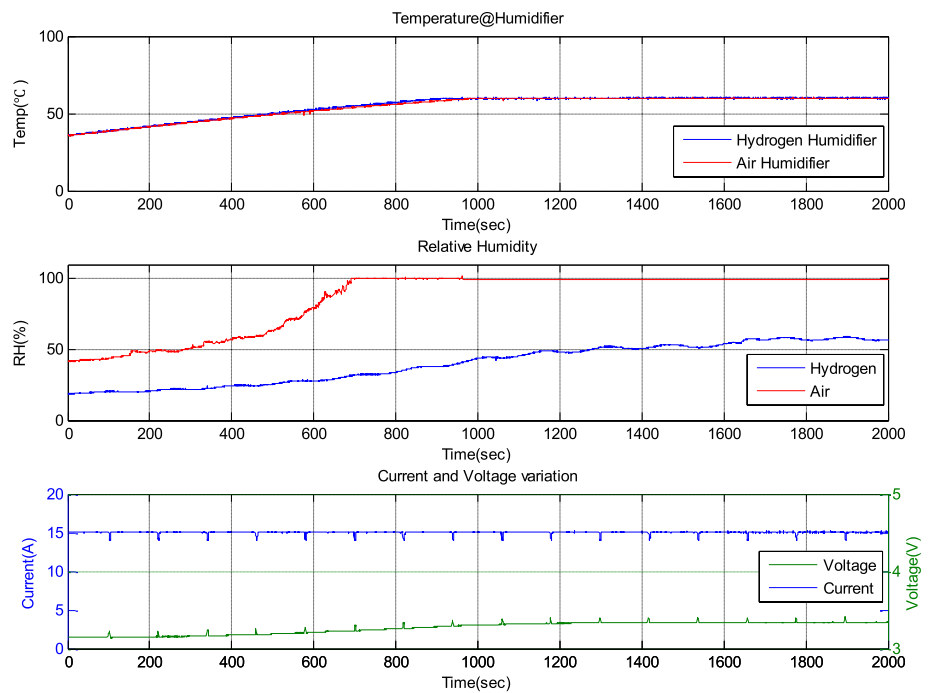**Fig. 9** Trends of several important conditions of test bench during State 2

Fig. 10 Variation of activation and membrane resistance of the stack during State 2

electrolyte membrane. Ionic conductivity is highly sensitive to the water content in the electrolyte membrane and if the ionic conductivity is reduced, this is shown to increase membrane resistance in the equivalent circuit. Polymer electrolyte membrane ionic conductivity as a formula can be represented as in Eq. (12) [10].

$$K = (0.5139\mu - 0.326) * \exp\left[1268\left(\frac{1}{303} - \frac{1}{T}\right)\right] \qquad (12)$$

$$\mu = 0.043 + 17.81h - 39.85h^2 + 36.0h^3 \qquad (13)$$

Equation (14) represents the resistance of the electrolyte membrane by using the thickness of the electrolyte membrane (t) and ionic conductivity (K) [10].

Table 6 Transition of the total model parameters during State 2

No. of sampled data	R_a	R_m
Experiment 1	0.0567	0.0121
Experiment 4	0.0558	0.0108
Experiment 8	0.0526	0.0091
Experiment 12	0.0525	0.0085
Experiment 15	0.0512	0.0082
Δ Total (%)	− 9.7	− 32.23

Table 7 Transition of the total model parameters during State 3

No. of sampled data	R_a	R_m
Experiment 1	0.0465	0.0082
Experiment 4	0.0535	0.0081
Experiment 8	0.0610	0.0079
Experiment 12	0.0687	0.0069
Experiment 14	0.0704	0.0069
Δ Total (%)	+ 51.40	− 15.85

$$R_m = \frac{1000 * t}{K} \qquad (14)$$

Based on the equation above, the ionic conductivity is a function of μ because the temperature of stack is fixed during this test. Since μ is a function of the relative humidity of reactants, eventually we can take ionic conductivity as a function of the relative humidity of reactants. If the relative humidity of reactants is lowered, μ and K are

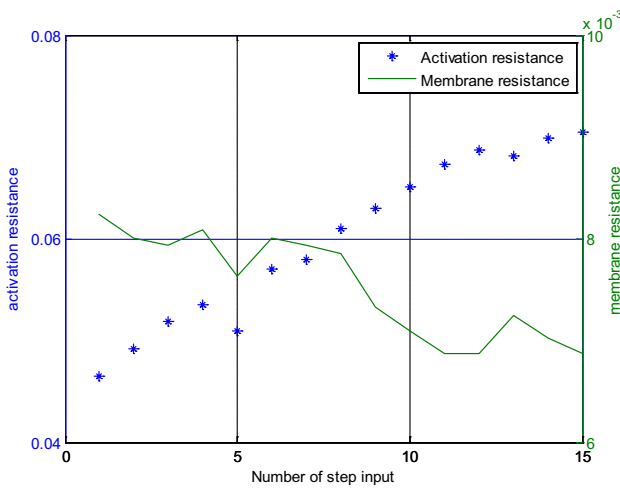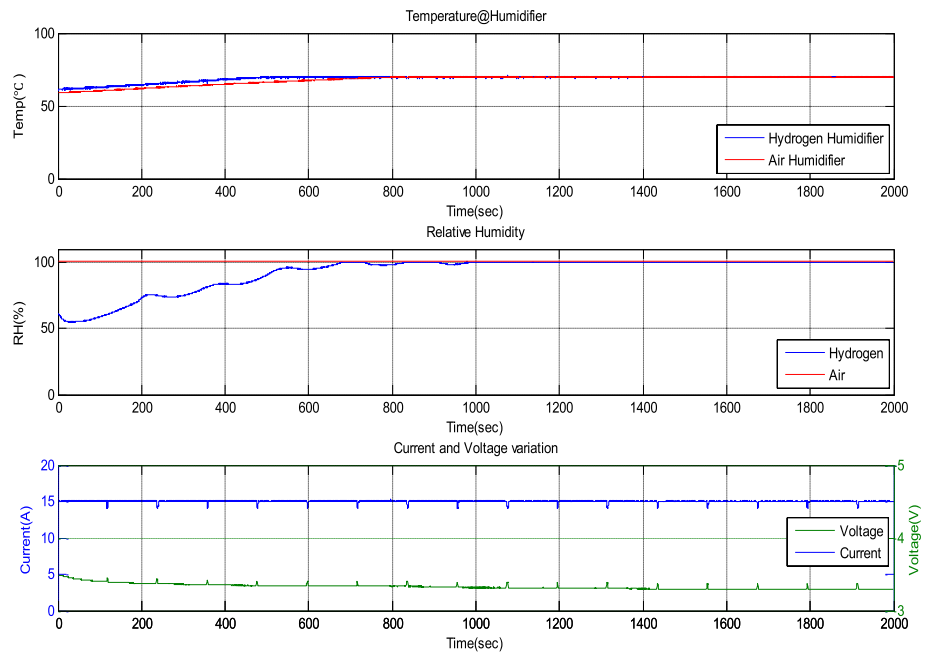**Fig. 11** Trends of several important conditions of test bench during State 3

Fig. 12 Variation of activation and membrane resistance of the stack during State 3
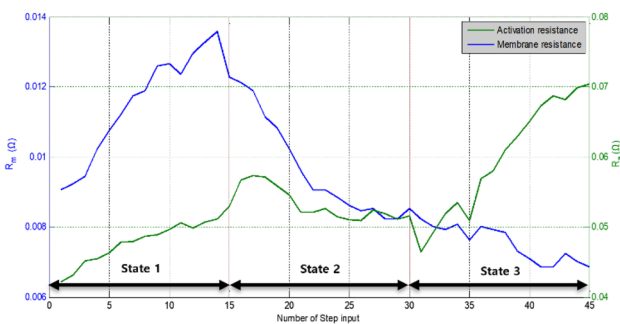

Fig. 13 Variation of activation and membrane resistances during the whole states

lowered together and this instance leads to an increase in membrane resistance.

4.2 Analysis of State 2

In State 2, the relative humidity is increased again in the inlet gas that is input to the cell component, thereby increasing relative humidity in the fuel and oxidant hydrate in the electrolyte membrane. In this regard, the membrane resistance is recovered as much as the initial state of State 1 as the hydration of electrolyte membrane in the PEMFC stack has recovered and it leads to a decline of membrane resistance based on Eqs. (12, 13, 14).

4.3 Analysis of State 3

The activation resistance has shown an increase in State 3 multiple-times that of the increase in membrane resistance. First of all, the membrane resistance showed a reduction during State 3; however, its slope is small compared to other states and does not fall much further from a certain level. To explain this phenomenon, the relationship between accumulations of water contents at GDL and membrane resistance should be investigated. The cause of this is found in [9] which explains that the membrane resistance converges to a constant value after passing the optimum point as the membrane hydration progresses. It can be seen that the tendency described in the paper is still present in this experiment.

Also, we can observe a change in activation resistance during State 3 and Eqs. (15) and (16) [10] show correlations among activation polarization represented by activation

resistance, exchange current density at cathode, and catalyst specific area at cathode because most portions of activation polarization are related to activation energy at the cathode.

$$V_{act} = \frac{R_u T}{nFa} * \ln\left(\frac{I + I_{in}}{I_0}\right) \qquad (15)$$

$$I_0 = I_{0,ref} A_c L_c \left(\left(\left(\frac{0.21\left(P - \O P_{H_2o,sat}\right)}{P}\right)\right)^{\frac{1}{2}} \right. $$
$$\left. * \exp\left[-\frac{E_c}{RT} * \left(1 - \left(\frac{T}{298.15}\right)\right)\right]\right) \qquad (16)$$

Since temperature in the PEMFC stack during the test is fixed and the other parameters are constant, (15) is a function of exchange current density I_0. This can be calculated by (16) as function of catalyst specific area A_C because other parameters are of constant value in this test. Thus, as accumulation of water contents at GDL proceeds, gradual reduction of catalyst specific area is achieved. If a catalyst-specific area is reduced, the V_{act} increases in (16). One can then conclude that congelation of water contents at GDL reduces catalyst specific area where reactants can make reaction, leading to a decline in exchange current density. Finally, reduced exchange current density brings about increased activation polarization (V_{act}) by increasing activation resistance in State 3.

5 Conclusions

Water management of PEMFC is a critical issue in PEMFC application for commercialization. For detecting PEMFC water balance, the SRA method has been discussed here. This method is based on R_m and R_a which are components of the PEMFC equivalent circuit. In this paper, an interesting finding is that it is possible to find R_m and R_a by using a simple step current consumption.

Also, the correlation between the variation of resistance values in equivalent circuit calculated by SRA and water balance conditions in PEMFC (dry-out and flooding) is assessed. Using this SRA method is not only a simple and convenient solution for monitoring water balance in PEMFC stack; it also has an advantage in on-board integration system for real time application because of its simple signal processing.

References

1. Onanena, R., Oukhellou, L., Côme, E., Candusso, D., Hissel, D., & Aknin, P. (2012). Fault-diagnosis of PEM fuel cells using electrochemical spectroscopy impedance. *IFAC Proceedings Volumes, 45,* 651–656.
2. Andreasen, S., Jespersen, J., Schaltz, E., & Kær, S. K. (2009). Characterisation and modeling of a high temperature PEM fuel cell stack using electrochemical impedance spectroscopy. *Fuel Cells, 9,* 463–473.
3. Webb, D., & Møller-Holst, S. (2001). Measuring individual cells voltages in fuel cell stacks. *Journal of Power Sources, 103,* 54–60.
4. Ramschak, E., Peinecke, V., Prenninger, P., Schaffer, T., Baumgartner, W., & Hacker, V. (2006). Online stack monitoring tool for dynamically and stationary operated fuel cell systems. *Fuel Cells Bulletin, 2006,* 12–15.
5. Fouquet, N., Doulet, C., Nouillant, C., Dauphin-Tanguy, G., & Ould-Bouamama, B. (2006). Model based PEM fuel cell state-of-health monitoring via ac impedance measurements. *Journal of Power Sources, 159,* 905–913.
6. Kim, J., Jang, M., Choe, J., Kim, D., Tak, Y., & Cho, B. (2011). An experimental analysis of the ripple current applied variable frequency characteristic in a polymer electrolyte membrane fuel cell. *Journal of Power Electronics, 11,* 82–89.
7. Steiner, N. Y., Hissel, D., Moçotéguy, P., & Candusso, D. (2011). Diagnosis of polymer electrolyte fuel cells failure modes (flooding and drying out) by neural networks modeling. *International Journal of Hydrogen Energy, 36,* 3067–3075.
8. Lebreton, C., Benne, M., Damour, C., Yousfi-Steiner, N., Grondin-Perez, B., Hissel, D., et al. (2015). Fault tolerant control strategy applied to PEMFC water management. *International Journal of Hydrogen Energy, 40,* 10636–10646.
9. Owejan, J. P., Gagliardo, J. J., Reid, R. C., & Trabold, T. A. (2012). Proton transport resistance correlated to liquid water content of gas diffusion layers. *Journal of Power Sources, 209,* 147–151.
10. Noh, Y., Kim, S., Jeong, K., Son, I., Han, K., & Ahn, B. (2008). Modeling and parametric studies of PEM fuel cell performance. *Transactions of the Korean Hydrogen and New Energy Society, 19,* 209–216.

Dong-Hoon Shin received the B.S and M.S degrees in mechanical engineering from Korea University of Technology and Education, Cheonan-Si, Korea, in 2010 and 2013, respectively. He is currently a doctoral student at Korea University of Technology and Education. His research interests include diagnosis and prognosis with applications to proton exchange membrane fuel cell, Lithium-ion battery.

Seung-Ryeol Yoo received his B.S in mechanical engineering from KAIST, Daejeon, Korea in 1990, his M.S degrees in mechanical engineering from POSTECH, Pohang, Korea in 1992, and his Ph.D. in mechanical engineering from Rensselaer Polytechnic Institute, Troy, NY USA in 2004. He is currently a professor at Korea University of Technology and Education. His research interests include diagnosis and control.

Young-Hyun Lee received the B.S, M.S (Diploma) and doctor degrees in electrical engineering from RWTH Aachen, Germany, respectively. He is currently a professor at Kangnam University, Korea. His research interests include diagnosis for proton exchange membrane fuel cell stack system and autonomous vehicle.